

Spontaneous Nanoparticle Dispersal in Polybutadiene by Brush-Forming End-Functional Polymers

James M. Hart,[†] Solomon M. Kimani,[†] Lian R. Hutchings,[†] Isabelle Grillo,[§] Arwel V. Hughes,^{||} Nigel Clarke,^{†,⊥} Victoria Garcia-Sakai,^{||} Sarah E. Rogers,^{||} Budhika Mendis,[‡] and Richard L. Thompson^{*,†}

[†]Department of Chemistry and [‡]Department of Physics, Durham University, Mountjoy Site, Durham DH1 3LE, U.K.

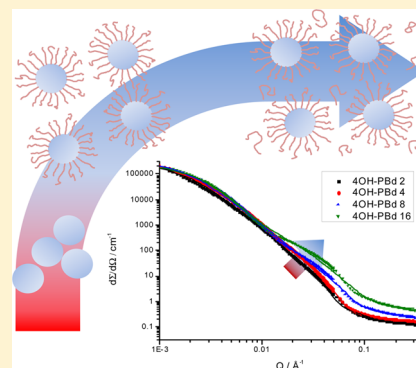
[§]Institut Laue-Langevin, 71 avenue des Martyrs, 38000 Grenoble, France

^{||}ISIS Pulsed Neutron Source, Rutherford Appleton Laboratories, Chilton, Didcot OX11 0QX, U.K.

[⊥]Department of Physics and Astronomy, The University of Sheffield, Hicks Building, Hounsfield Road, Sheffield S3 7RH, U.K.

Supporting Information

ABSTRACT: A masterbatch additive for the enhanced dispersal of bare silica nanoparticles in polybutadiene is demonstrated using tetrahydroxyl end-functional polybutadienes (“4OH-PBd”). Neutron reflectometry and small-angle neutron scattering (SANS) confirm the efficient end-adsorption of 4OH-PBd at a planar silica interface and silica particle interfaces of increasing complexity. SANS on well-defined model Stöber silica nanospheres in polybutadiene revealed spontaneous 4OH-PBd adsorption, forming a “shell” around the silica nanospheres. Analysis using a core–shell fractal model showed that the extent of adsorption was consistent with the interfacial excess determined by NR. The utility of 4OH-PBd additives to disperse silica nanoparticles was explored rigorously for a range of compositions and additives. Successful silica nanoparticles dispersal was evident from a reduction in the correlation length of the largest structures in the mixture and increase in fractal dimension, ascribed to a breakdown of percolating nanoparticle aggregates to smaller, denser clusters. A critical surface concentration of 4OH-PBd is identified, which is necessary to inhibit particle–particle aggregation. Scaling theory analysis over four different molecular weights of 4OH-PBd and several concentrations indicates that the transition in silica dispersal coincides closely to the transition from “mushroom” to “brush” scaling of the adsorbed 4OH-PBd. Rheological testing on the same composites yielded a dramatic decrease in moduli with increasing 4OH-PBd: silica ratio, particularly at low frequencies, which is consistent with the breakdown of large aggregates evidenced by SANS. Additives of this type could significantly simplify the processing of nanocomposites by eliminating the need for prior functionalization of the nanoparticles.



INTRODUCTION

Composite and nanocomposite materials offer significant advantages over unfilled polymers, notably in mechanical, thermal, and optical properties, with greater strength, resistance to heat, and photodegradation being among these desirable properties. These benefits are perhaps best exemplified by the very successful use of filler particles in car tires. Nevertheless, considerable challenges remain in simultaneously optimizing different aspects of performance, such as durability, wet grip, and energy efficiency. Energy efficiency is substantially compromised by strain softening (Payne) and hysteresis (Mullins) effects, which are prevalent in filled rubbers.^{1–4} Remarkably for this mature technology, there is still debate over the exact cause of reinforcement and associated phenomena such as energy dissipation, although it is apparent that the distribution of filler particles and their interactions with each other and the surrounding polymer are of central importance.

For other applications, controlling nanoparticle dispersion in polymers for magnetic inks and data storage is a current challenge,⁵ and polymer reinforcement, e.g. with graphene-

based fillers, requires control over the polymer–particle interface.⁶ Given these drivers, there is therefore of considerable interest in controlling the dispersion and organization of filler particles in rubbery polymers and the relationship between structure and performance.

It is established that modifying the surface of nanoparticles to render them more compatible with a polymer matrix is an important step toward achieving their dispersal. This analogous process is well-known for colloidal solutions, and the use of an adsorbed layer to achieve steric stabilization has been documented since the 1970s.⁷ For nanoparticle dispersal in polymers this approach to make nanocomposites is still a developing field. Notably, Corbierre et al.⁸ report the use of thiol end-capped polymers to disperse gold nanoparticles. Successful dispersal required the matrix to wet the adsorbed stabilizing layer, which necessitated either a low molecular

Received: October 22, 2015

Revised: January 21, 2016

Published: February 2, 2016

weight matrix relative to the adsorbing polymer or a relatively low grafting density such that some voids on the surface were present. As the formation of a percolating filler structure is thought to reinforce a composite, disruption of this process should cause in considerable changes of material properties.^{9,10} Reports have noted the effects of structure formation and disruption on composite behavior before. Jouault et al.¹¹ have used SANS and rheology to explore the fractal properties of silica in PS homopolymer. Interestingly, they observed significant reinforcement at a silica volume fraction of 0.066, which is much lower than volume fraction required to make a continuous network. Baeza et al.^{12,13} have also combined scattering and rheology to silica SBR (styrene–butadiene rubber) nanocomposites. In the absence of polymer functionalization, other than terminal silanol groups on the SBR, small clustered aggregates with a fractal dimension of ~ 2.4 were observed. Using deuterium labeling and reactive functional groups, the same group demonstrated a reduction in aggregate size with grafting, which appeared to require a critical minimum grafting density.¹³

Methods such as rheology are excellent for the determination of macroscopic properties; however, there is little direct information gained about the microscopic phenomena. Neutron scattering, on the other hand, provides details about phenomena on the molecular to microscopic level, but the difficulty lies in linking these to macroscopic properties. The combination of neutron scattering and rheological techniques is therefore a powerful approach to study both the micro- and macroscopic regimes to investigate the reinforcement of polymer nanocomposites and gain insight into underlying molecular phenomena. In this article we explore for the first time the dispersal of silica nanoparticles using a series of well-defined end-functional polymers of systematically varying molecular weight and composition. By linking neutron reflectometry to examine the structure of interfacially adsorbed layers to SANS, which is sensitive to nanoparticle distribution as well as the adsorbed layer structure, we isolate these factors and can resolve the impact of grafting density on nanoparticle dispersion. Finally, rheometry carried out on the same samples that were the subject of the SANS experiment provides the relationship between nanoscale dispersal and macroscopic properties.

METHODS

Polymers. The synthesis and characterization methods have been previously reported¹⁴ and will only be summarized here. Briefly, the end-functional 1,4-polybutadiene (4OH-PBd, Figure 1) used in these experiments was synthesized by anionic polymerization of butadiene, which was then end-capped with a tetrahydroxyl functional group. End-capping was carried out by a click reaction with at least 95% efficiency, as determined by NMR. Unfunctionalized perdeuterated

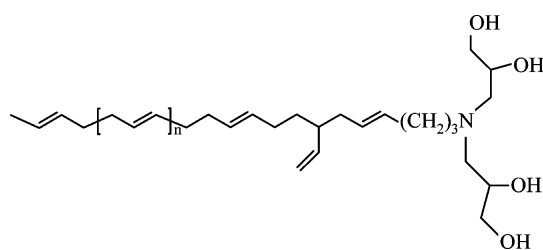


Figure 1. Chemical structure of the end-functionalized polybutadiene (4OH-PBd).

polybutadiene was prepared by standard living anionic polymerization methods. Molecular weights were determined by size exclusion chromatography, and radii of gyration (R_g) values were calculated according to the scaling relation $R_g = kM_w^{1/2}$ for hydrogenous 1,4-polybutadiene.¹⁵ Sample codes, molecular weight data, and degree of end-capping data for the polymers used in this work are summarized in Table 1.

Table 1. Summary of Characteristics of 4OH End-Functional and Nonfunctional Perdeuterated Polybutadienes

sample code	M_n (kg mol ⁻¹)	M_w (kg mol ⁻¹)	% end-capping	R_g (Å)
4OH-PBd-5k	6.05	6.40	97	31
4OH-PBd-10k	9.80	10.3	96	39
4OH-PBd-15k	17.4	18.5	97	52
4OH-PBd-20k	22.5	23.6	95	59
d ₆ -PBd-90k	88.0	90.6	n/a	109
d ₆ -PBd-140k	138.0	140.8	n/a	136

Silica Nanoparticles. Silica nanopowder (CAS #7631-86-9, lot 4830-012711) was purchased from Nanostructured and Amorphous Materials Inc. (Houston, TX) and used as received. Additionally, silica spheres were prepared in-house from tetraethyl orthosilicate using the Stöber process at room temperature.¹⁶ Characterization of these particles in aqueous solution by dynamic light scattering given as Supporting Information S.I.1 found the average radius was 450 Å (800–1000 Å diameter), and subsequent TEM analysis, using a JEOL 2100F FEG TEM, confirmed that they were nearly monodisperse spheres (Figure 2). TEM analysis of the nanopowder sample further confirmed the approximate size of the particles, quoted as 800 Å diameter, which in this case are much less regular in shape. For clarity hereafter, we refer to the commercial nanopowder sample as “silica nanoparticles” and the Stöber process sample as “silica nanospheres”. We note that for both silica materials the average radius is more than 8 times the statistical step length of polybutadiene;¹⁷ therefore curvature effects on the adsorbed brush layer form are expected to be negligible.¹⁸

Neutron Reflectometry (NR). Thin (~ 750 Å) polybutadiene blend films were prepared by spin-casting from toluene solutions onto clean silicon blocks of 50 mm diameter and 5 mm thickness. Silicon blocks were thoroughly cleaned by first immersing in toluene, then drying, and finally immersing in permanganic acid to remove any last traces of organic impurities. The absence of organic contaminants was verified by ellipsometry, which confirmed the presence of a silicon oxide layer of 20–30 Å on the block surface. Here, this feature is important because it means that the silicon oxide block surface is the 1-dimensional analogue for the silica nanoparticles which are the main focus of this work. The functional polymer, 4OH-PBd-20k, and matrix polymer, d₆-PBd-90K, were codissolved in the desired proportions to determine the average film composition. Neutron reflectometry was carried out on the SURF reflectometer, ISIS pulsed neutron and muon source, Rutherford Appleton Laboratories, Chilton, UK. Specular reflectivity was measured at incident angles of 0.25°, 0.65°, and 1.5°, which enabled $R(Q)$ to be determined from $0.008 < Q/\text{Å}^{-1} < 0.35$, so covered the range from before the critical edge to a point at which the signal became indistinguishable from the background. Here, Q is the scattering vector, defined as $Q = (4\pi/\lambda) \sin(\theta/2)$, where λ is the de Broglie wavelength of the neutron and θ is the scattering angle.

Small-Angle Neutron Scattering (SANS). A composite sample comprising 24:20:56 (w/w) ratio of Stöber silica spheres, 4OH-PBd-20k polymer, and perdeuterated 1,4-polybutadiene (d₆-PBd-140 K) components was mixed by solvent casting in toluene. The sample environment was a quartz window cell, 13 mm diameter with a 1 mm spacer, at standard temperature and pressure. Measurements were performed on the SANS2D instrument at ISIS pulsed neutron and muon source. The incident beam was collimated to 6 mm with the front and rear detectors at 12 and 6 m from the sample, respectively. This set up enabled a large Q range ($0.0015 < Q/\text{Å}^{-1} < 0.85$) to be captured in a single measurement. Data were corrected and reduced to

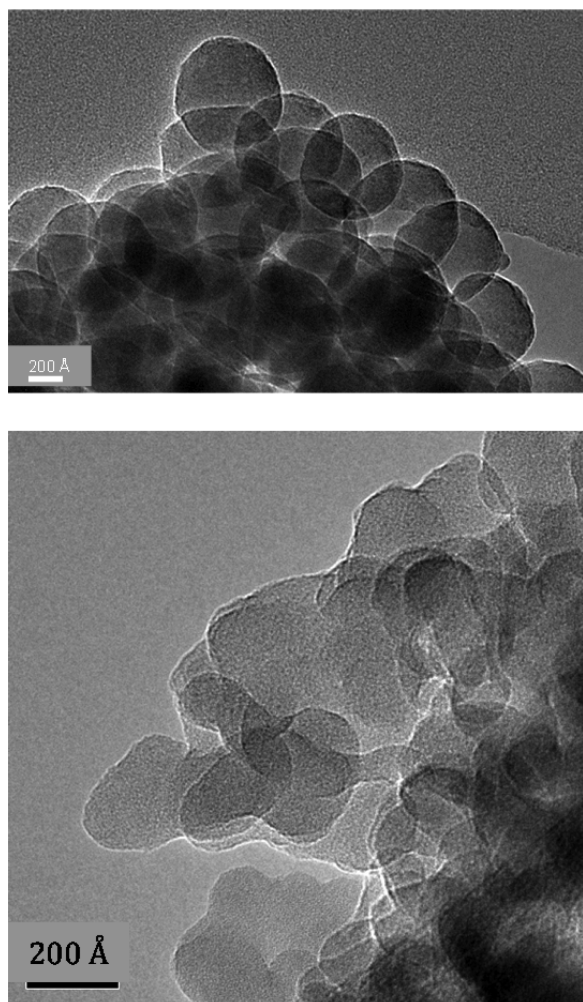


Figure 2. TEM image of Stöber silica nanospheres (top) and silica nanopowder (bottom). In both cases the scale bar corresponds to 200 Å.

an absolute scale by comparison with a polystyrene standard using Mantid software.^{19,20}

A range of similar samples for SANS scattering were also prepared at two loadings of commercial silica nanoparticles at (5 or 20% (w/w)), and various loadings (1–16% w/w) of each 4OH-PBd additive (approximately 5k, 10k, 15k, and 20k) were used. In this case the samples were simply prepared by manual mixing of the dry ingredients until the sample appeared to be completely homogeneous. The bulk matrix was perdeuterated polybutadiene *d*₆-PBd-90. Samples were characterized on the D11 diffractometer, Institute Laue Langevin, Grenoble, France, using the same cell and conditions as for the SANS2D experiment. In order to capture a similar *Q*-range to SANS 2d, three detector distances (1.2, 8, and 39 m) were used. Data were scaled to absolute values (partial differential scattering cross section/cm^{−1}) using the water cross section with LAMP software.

Rheology. Following structural investigation by small-angle neutron scattering, the mechanical properties of the same samples were carried out by oscillatory shear rheometry using 8 mm parallel plate geometry. Initial strain sweeps were carried out to ensure that measurements were confined to the linear viscoelastic (LVE) region with a maximum strain of 1%. The primary mode of measurement was a series of frequency sweeps at various temperatures using an AR-2000 rheometer. Data were shifted to 20 °C using the Williams–Landel–Ferry time–temperature superposition.²¹

RESULTS

1D Depth Profile. Specular neutron reflectivity data were fitted to scattering length density (SLD) profile using Motofit Software running on Igor.²² Constrained parameters were the upper and lower SLD of the polymer film components, which were held at 6.61 and $0.5 \times 10^{-6} \text{ Å}^{-2}$, respectively.

The NR data and fit for a blended film comprising 16% 4OH-PBd-20k in *d*₆-PBd-90K are shown in Figure 3, along

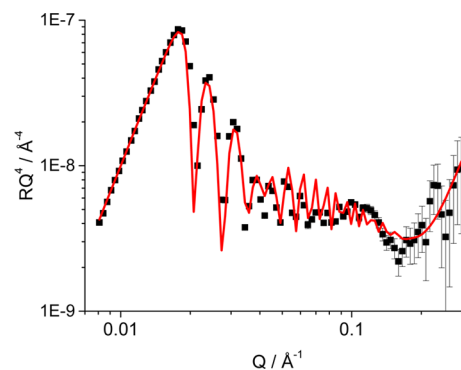


Figure 3. Neutron reflectivity data 16% 4OH-PBd-20k/dPBd-90K film on silica substrate (black) with fitted scattering curve (red).

with the best fit that could be obtained for a simple 2 polymer layer model that allowed for a diffuse interface between the polymer layers. Data are presented as RQ^4 to remove the Q^{-4} dependence of $R(Q)$ over the main fitting region of interest. Even this relatively simple model, in which the key variables are the thickness and scattering length density of each layer and the width of the interface, captures the data well. The profile in scattering length density corresponding to this fit is shown in Figure 4, and the corresponding volume fraction profile for the

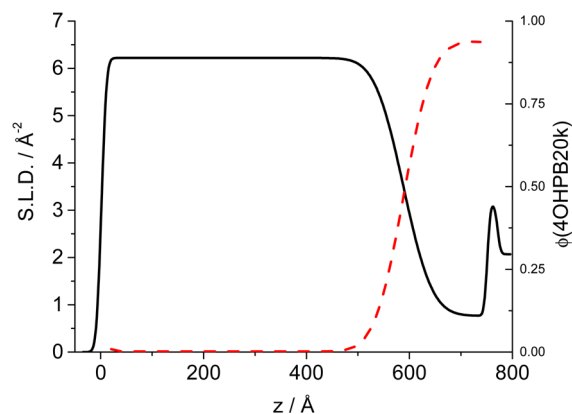


Figure 4. Calculated depth profiles for neutron scattering length density (black) and volume fraction of 4OH-PBd-20k (red) from the reflectivity data.

end-functional polymer is presented on a secondary axis for clarity. The NR results confirm the observation from our earlier work¹⁴ that the tetrahydroxyl end-functional polymer adsorbs very strongly to silica surfaces, and in fact our measurement suggests that almost all of the end-functional polymer is adsorbed the substrate interface and very little functional polymer is dispersed in the bulk of the film. The adsorbed layer appears to be almost pure with $\phi(4\text{OH-PBd}20\text{k})$ reaching a limiting value of approximately 0.9. The small peak in SLD at

approximately 760 Å depth corresponds to the silicon oxide layer at the substrate interface.

SANS data for the silica nanosphere dispersion were fitted with SASview software using a model of free and aggregated polydisperse core–shell particles and a Debye term to account for interchain scattering between deuterated and hydrogenous

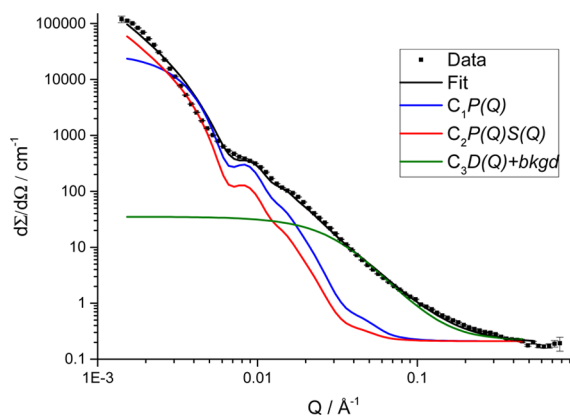


Figure 5. Small-angle neutron scattering data for 24% Stöber silica, 20% 4OH-PBd-20k, and 56% d_6 -PBd-140 K composite (data); best fit (black) is for a combination of free particles (blue) and fractal aggregates (red) with Debye and background terms (green).

polybutadienes. Data and fit are shown in Figure 5, and the fitting model has the general form given by eq 1

$$d\Sigma/d\Omega = I(Q) = \text{bkgd} + C_1P(Q) + C_2P(Q)S(Q) + C_3D(Q) \quad (1)$$

where bkgd is the background scattering, $P(Q)$ is the particle factor for core–shell spherical particles, $S(Q)$ is the structure factor, $D(Q)$ is the Debye scattering for free polymer chains, and C_i are the weightings of each contribution to the scattering.

Silica Nanosphere Filled PBd. Experimental SANS data obtained on Sans2d for 20% silica nanospheres in a mixture of multihydroxy end-functional polybutadiene and perdeuterated polybutadiene are presented in Figure 5. The strong scattering at very low Q is largely due to the silica particles (or their aggregates) which are likely to be coated with an adsorbed layer of 4OH-PBd-20k, and the weaker scattering at high Q ($>0.1 \text{ \AA}^{-1}$) is likely to be due to Debye scattering from intermixed deuterated and hydrogenous polybutadiene.

The particle form factor is given by

$$P(Q) = \frac{1}{V_s} \left[3V_c(\rho_c - \rho_s) \frac{\sin(Qr_c) - Qr_c \cos(Qr_c)}{(Qr_c)^3} + 3V_s(\rho_s - \rho_{\text{solv}}) \frac{\sin(Qr_s) - Qr_s \cos(Qr_s)}{(Qr_s)^3} \right]^2 \quad (2)$$

where ρ_c and ρ_s are the scattering length densities of the shell of adsorbed 4OH-PBd and silica sphere, respectively; r_c , r_s , and V_c , V_s are the radii and volumes of these components. The fractal structure factor has the form

$$S(Q) = \frac{D\Gamma(D-1) \sin((D-1) \tan^{-1}(Q\xi))}{(Qr_c)^D \left(1 + \frac{1}{Q^2\xi^2}\right)^{(D-1)/2}} \quad (3)$$

where ξ is the correlation length, Γ is the gamma function, and D is the fractal dimension of the aggregate. The Debye factor has the usual form

$$D(Q) = \frac{2(e^{-(QR_g)^2} + (QR_g)^2 - 1)}{(QR_g)^4} \quad (4)$$

where R_g is the radius of gyration associated with the blend polymer chains that are not adsorbed to the silica surface and C_3 is a scaling term.

The core–shell form factor and fractal structure factor were used as calculated by Guiner and Teixeira, respectively.^{23,24} Scattering length densities were held at the calculated values of $6.61 \times 10^{-6} \text{ \AA}^{-2}$ for the perdeuterated polybutadiene, $0.5 \times 10^{-6} \text{ \AA}^{-2}$ for the end-functional polybutadiene, and $3.7 \times 10^{-6} \text{ \AA}^{-2}$ for the silica spheres. Silica core radii values, correlation length, and fractal dimension were varied with bounds to prevent unphysical results. Polymer shell thickness was tied between the particle sizes but allowed to vary otherwise. Scaling between the model sections was performed manually.

Silica Nanoparticle Dispersions. The same fractal scattering model was used to fit the SANS data for the silica nanoparticle dispersions, for which typical data and fits are shown in Figure 6a. For these samples the model captures the

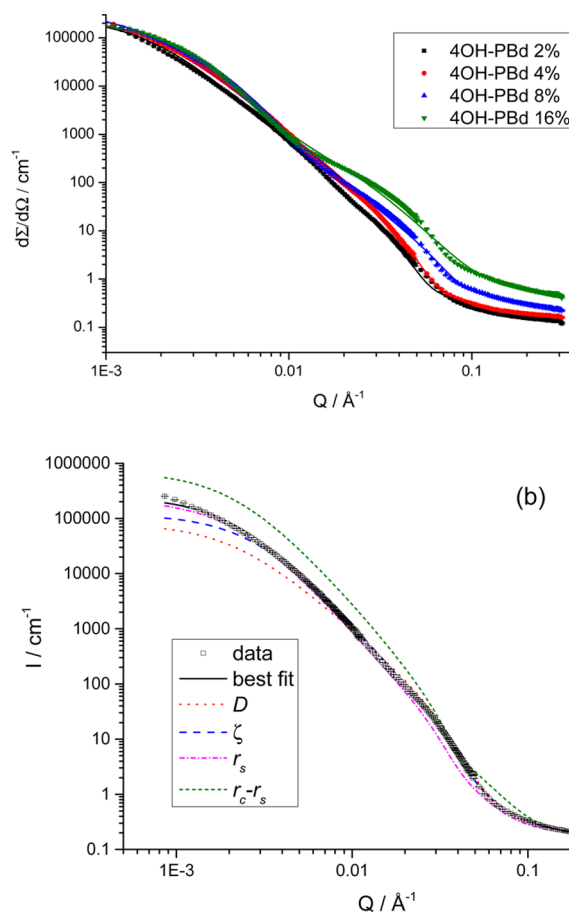


Figure 6. (a) SANS data and fits for 5% silica nanoparticle samples with various 4OH-PBd-5k loadings. (b) Influences of key fitting parameters on $I(Q)$: fractal dimension 2.81–2.5 (dotted red); correlation length from 4500 to 3500 Å (long-dash blue); particle radius from 390 to 500 Å (dash-dot magenta); layer thickness from 57 to 150 Å (short-dash green).

experimental data very well, and the solid lines for the fits are almost obscured by the experimental data. SLD were constrained as previously, while particle radius, shell thickness, correlation length, and fractal dimension were allowed to vary with reasonable bounds. Correlation length and particle radius were found to decrease, and the fractal dimension increased with increasing 4OH-PBd content. These changes in the model were observable as qualitative changes SANS data, namely, the increasing bulge around 0.04 \AA^{-1} and the decrease in low Q slope with end-functional polymer, which are apparent in Figure 6. Figure 6b shows the influence of each of the fitted parameters on a typical set of SANS data for these mixtures. It is clear that each parameter has a distinct impact on $I(Q)$. The fitted parameters for the nanoparticle dispersions are summarized in Table 3. Here, the sample code "XSi Y 4OH-PBd-Z k" indicates a mixture of X% (w/w) silica in Y% (w/w) 4OH-PBd of molecular weight Z kg/mol and $100 - X - Y$ % (w/w) d_6 -PBd-90k. Although there is some scatter in the results, several clear trends are apparent, namely, that with increasing concentration of 4OH-PBd additive, correlation length, ζ , tends to decrease, fractal dimension D tends to increase, and there are systematic shifts in the weighting factors indicating the increased prevalence of smaller particles. Plots of correlation length, fractal dimension, and weighting factors for 4OH-PBd-15k are shown in Figure 7 to illustrate these trends.

From the rheological tests (Figure 8a), the combination of d_6 -PBd-90k matrix and 4OH-PBd-20k polybutadienes results in an averaged modulus between them. The effect of the addition of 5% silica is shown in Figure 8b. At this relatively modest loading, the impact of the silica on the elastic moduli is rather similar to that of adding the 4OH-PBd-20k, but interestingly, when both are added together, there is no further increase. However, 20% silica addition (Figure 8c) increases the viscoelastic moduli considerably and almost eliminates the frequency dependence at low frequency. The orders of magnitude increase in storage modulus is nonlinear with regard to the proportion of silica in the sample, in agreement with literature;^{3,4,25} in other words there is significant reinforcement. The addition of end-functional polymer induces a marked decrease in both the 5% and 20% composite sample moduli and notably restores the frequency dependence of the moduli, signaling viscous rather than elastic dominated behavior at low frequency.

DISCUSSION

Interfacial Structure. NR analysis revealed a hydrogenated 4OH-PBd-20k layer of 162 \AA thickness and a sharp interface next to the silica substrate. The magnitude of the surface excess is in agreement with previous examinations of this polymer system by elastic recoil detection.¹⁴ Additionally, the neutron reflectometry can also resolve that the shape of the excess concentration profile is consistent with that of a brushlike layer.²⁶ If the adsorption of the end-functional polymer were due to the affinity of the entire chain, rather than just a single end-group to the silica surface, a more exponentially decaying profile would be expected.^{27–29} This result gives us further confidence that the mode of adsorption is appropriate for a polymer chain required to enable dispersion of silica particles in polybutadiene, although the near exclusion of matrix from the adsorbed layer indicates that autophobic dewetting might be expected if similar grafting densities are achieved in the bulk.⁸ Although blends of deuterated and hydrogenous polybutadienes are known to phase separate at high molecular weight,³⁰

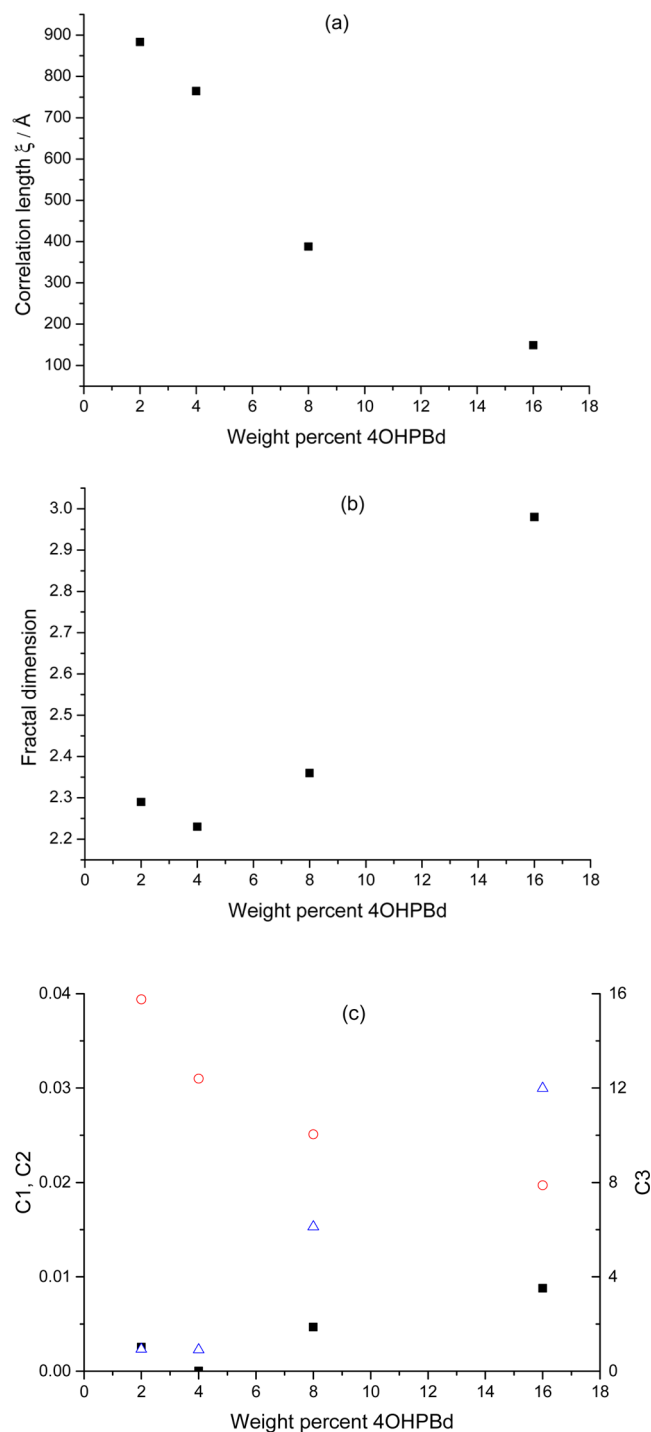


Figure 7. Dependence of fitted parameters for 20% silica composite at different concentrations of 4OH-PBd-15k additive: (a) correlation length, (b) fractal dimension, and (c) scale factors: C_1 (black solid squares), C_2 (red open circles), and C_3 (blue open triangles).

this cannot explain the observed result as the mean molecular weight of the deuterated and hydrogenous polybutadienes is orders of magnitude below this threshold.

Bulk Structure. Model Silica Nanosphere Composites. The SANS data for this model nanocomposite system provide additional evidence to support the neutron reflectivity data as the shell thickness (Table 2) calculated from $r_c - r_s$ is in good agreement with the layer thickness measured by NR. Moreover, the spherical particle radius of $405 \pm 61 \text{ \AA}$ obtained by SANS

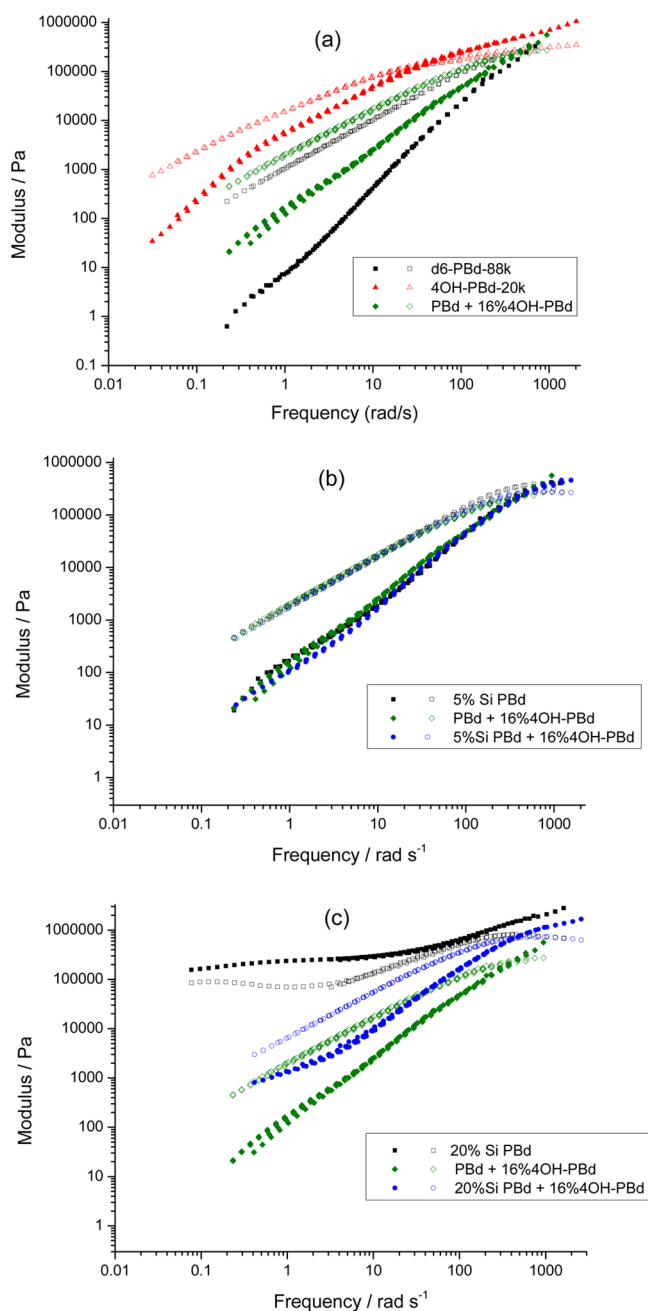


Figure 8. Storage (closed) and loss (open) moduli of WLF shifted frequency sweeps of blends (a), 5% (b), and 20% (c) composite samples.

Table 2. SANS Model Parameters for Stöber Silica Nanospheres in a Polybutadiene Blend, Corresponding to Model Fit in Figure 5

parameter	value
radius, $r_s/\text{Å}$	405 ± 61
shell thickness $r_c - r_s/\text{Å}$	173 ± 24
fractal dimension D	2.20 ± 0.02
correlation length $\xi/\text{Å}$	4400 ± 3100
C_1 free particle scale	$(11.0 \pm 0.05) \times 10^{-3}$
C_2 aggregate scale	$(4.13 \pm 0.03) \times 10^{-3}$
C_3 Debye scale	35.5
4OH-PBd-20k $R_g/\text{Å}$	58 ± 1
d6-PBd-140k $R_g/\text{Å}$	134 ± 1

was consistent with the hydrodynamic radius (450 Å) determined by ancillary dynamic light scattering experiments in aqueous dispersions of the nanospheres. The fractal core-shell scattering term suggests the presence of aggregated silica in the system with a fractal dimension of 2.2. The determined correlation length of the order of 4400 Å has a very large associated uncertainty. The correlation length is clearly finite, yet significantly larger than the individual particle size; therefore, it indicates some degree of silica nanosphere association into small aggregates. The high uncertainty reported on the correlation length is likely due to a large range of aggregate sizes, possibly going beyond the range probed by the instrument. Given this variation in size, the aggregates are probably the result of incomplete dispersal of the starting silica nanospheres rather than from aggregation in solution, which would be expected to yield a narrower size distribution and a larger apparent particle size determined by DLS. Overall, this model provides a reasonable physical situation for the composite system in question with a mixture of free and aggregated particles producing the calculated scattered intensity. The result from this well-defined system justifies the use of a core-shell and fractal model for the analysis of other less defined silica composites.

Nanoparticle Dispersions. There are several noticeable trends in the SANS data for the nanoparticle dispersion, exemplified in Figure 7. First, the absolute values of correlation length are significantly smaller than were recorded for the silica nanospheres, and all fall well within the range of the D11 diffractometer. In other words, the nanoparticles appear to be more dispersed than the silica nanospheres, which is likely due to the smaller specific surface area of these somewhat larger particles. Furthermore, there is a notable decrease in correlation length with end-functional polybutadiene content. This trend appears to be universal regardless of end-functional chain length (Table 3), although weaker in the 5% silica composite. Low polymer content and the bare silica control samples yield a fractal dimension of about 2.2; this is similar to the results for the nanosphere aggregates and to the reported value from reaction limited aggregation.³¹

Also of note is the shift between the free particle and aggregate scaling factors, C_1 and C_2 , with end-functional polymer content (Figure 7c). Although the exact nature of this shift varies between sample sets (Table 3), the general trend of increasing free particle scaling and a corresponding decrease in aggregate scaling is found throughout. As the scaling term is related to the relative concentration of a component in the system, a conclusion can be made for the dispersal of the silica aggregate structures by the addition of the end-functionalized polymer. At higher loadings of 4OH-PBd, the scale factor C_3 for the weighting of the Debye scattering term increases substantially, as would be expected for increasing mixing between deuterated and hydrogenous polymers. This may be due to the excess 4OH-PBd being dispersed throughout the matrix, rather than forming a pure adsorbed layer on the silica surface from which the matrix is excluded.

The results also show that there is a trend of increasing dimensionality toward 3 with the end-functional polymer content, as seen in Figure 7b. At first glance an increase in fractal dimension yields a more compact arrangement; however, it is important to couple this with the decrease in correlation length, ξ , and the shift in scaling factors. The smaller more compact structure observed at high 4OH-PBd concentrations is likely the primary aggregate structure that forms the larger

Table 3. Fit Parameters for SANS Experiments on Nanoparticles in PBd^a

sample code	r_s (Å)	$r_c - r_s$ (Å)	ξ (Å)	D	C_1	C_2	C_3	Debye R_g (Å)
20Si 0 4OH-PBd	51	0.0	1160	2.20	0	0.133	0	38
20Si 2 4OH-PBd-5k	68	12	810	2.24	1.51×10^{-6}	0.0605	6.13×10^{-6}	30
20Si 4 4OH-PBd-5k	38	22	430	2.45	6.94×10^{-8}	0.0306	8.68×10^{-4}	30
20Si 8 4OH-PBd-5k	23	25	180	2.85	5.16×10^{-3}	0.0138	3.19	30
20Si 16 4OH-PBd-5k	29	13	200	2.69	0.0147	0.0394	1.99	30
20Si 4 4OH-PBd-10k	66	20	790	2.14	4.90×10^{-7}	0.0719	0	38
20Si 8 4OH-PBd-10k	34	28	200	2.85	2.23×10^{-3}	0.0198	5.15	38
20Si 16 4OH-PBd-10k	29	20	180	2.79	6.11×10^{-3}	0.0519	2.27	38
20Si 2 4OH-PBd-15k	74	16	880	2.29	2.54×10^{-3}	0.0394	0.933	47
20Si 4 4OH-PBd-15k	66	27	760	2.23	9.78×10^{-6}	0.031	0.907	47
20Si 8 4OH-PBd-15k	46	50	390	2.36	4.67×10^{-3}	0.0251	6.12	47
20Si 16 4OH-PBd-15k	34	27	150	2.98	8.79×10^{-3}	0.0197	11.99	47
20Si 4 4OH-PBd-20k	65	35	720	2.22	1.95×10^{-6}	0.0249	3.74	58
20Si 16 4OH-PBd-20k	33	21	160	3.00	8.59×10^{-8}	0.0467	13.2	58
5Si 2 4OH-PBd-5k	29	24	550	2.80	1.31×10^{-3}	4.95×10^{-3}	0.169	30
5Si 4 4OH-PBd-5k	18	34	560	2.69	1.70×10^{-3}	2.08×10^{-3}	0.252	30
5Si 8 4OH-PBd-5k	21	10	550	2.77	0.0200	6.82×10^{-3}	0.2	30
5Si 16 4OH-PBd-5k	30	76	390	3.00	0.0258	5.12×10^{-3}	8.06	30
5Si 2 4OH-PBd-10k	30	23	620	2.76	5.62×10^{-9}	4.75×10^{-3}	0.0294	38
5Si 4 4OH-PBd-10k	36	34	570	2.66	1.31×10^{-4}	7.04×10^{-3}	0.246	38
5Si 8 4OH-PBd-10k	27	14	430	2.83	9.87×10^{-3}	5.49×10^{-3}	0.306	38
5Si 16 4OH-PBd-10k	32	12	540	2.78	0.0512	8.25×10^{-6}	1.15	38
5Si 2 4OH-PBd-15k	27	33	650	2.77	1.69×10^{-7}	1.67×10^{-3}	1.03	47
5Si 4 4OH-PBd-15k	31	45	540	2.73	3.12×10^{-4}	2.27×10^{-3}	2.04	47
5Si 8 4OH-PBd-15k	34	33	330	2.93	3.25×10^{-3}	6.56×10^{-3}	1.15	47
5Si 16 4OH-PBd-15k	29	29	420	2.82	0.0336	5.42×10^{-3}	6.64	47
5Si 1 4OH-PBd-20k	49	33	1050	2.56	2.53×10^{-6}	3.73×10^{-3}	0.60	58
5Si 2 4OH-PBd-20k	31	41	610	2.79	1.02×10^{-4}	1.55×10^{-3}	2.34	58

^aSample code: x Si y 4OH-PBd- z denotes $x\%$ w/w silica in $y\%$ w/w 4OH-PBd z (nominal kg/mol) in $(100 - X - Y)\%$ w/w dPBd.

agglomerates observed at lower concentrations. This suggests a change from an aggregated cluster system toward a particulate system closer to hard sphere dispersion. Lin et al.³² report that the fractal dimension of colloidal aggregates increases from 1.8 (or 1.86)³³ to 2.10 ± 0.05 ³¹ as the aggregation mechanism switches from diffusion limited to reaction limited. In other words, an activation energy barrier to aggregation, such as might be expected for the presence of a dense brush layer, should lead to more compact aggregates with a higher fractal dimension. Although the scaling exponents do not agree with our values, this is likely to arise from the fact that the silica particles are not aggregated from an initially homogeneous distribution, but rather are being separated by a mixture of shearing during melt mixing and some degree of adsorption of the 4OH-PBd, when available. Nevertheless, the concept of a barrier to aggregation leading to smaller more condensed aggregations with a higher fractal dimension remains sound.

Further analysis was performed by the comparison of the data in regard to the chain surface area (Figure 9). The available total surface area was calculated by treating the silica nanoparticles as ideal spheres with a set radius. The chain population was determined from the molecular weight and was divided by the silica surface area to achieve the chain surface area. For the 20% silica composites (Figure 9b), this method produces a noticeable step in correlation length at approximately 750 \AA^2 . This step is less visible in the 5% composite; however, there is insufficient data to disprove its existence as most of the points are below the step in the 20% silica data.

This observed step in correlation length can be ascribed to the dispersion of the silica aggregates in the composite and the

formation of a steric layer to stabilize the system. The correlation lengths at concentrations lower than the step, being of similar magnitude to that of the bare silica composite, 1160 Å ("20 Si 0 4OH PBd", Table 3), support this idea. The presence of the step itself suggests there is a critical surface concentration of the end-functional chains that needs to be reached before the dispersal of the silica is energetically favorable, and that it is independent of chain length.

It is interesting to consider the steplike transition in behavior in terms of the normalized grafting density of polymer brushes. Aubouy et al. used scaling models to calculate a phase diagram for end-adsorbed polymer chains as a function of grafting density and molecular weight.³⁴ When the molecular weight of the matrix is equal to (or somewhat exceeds) that of the adsorbing species, no difference in adsorbed species brush height is expected with normalized grafting density until this reaches a value of $\sigma > N^{-1/2}$. Results for this analysis are presented in Figures 10a and 10b for 5% and 20% silica, respectively. Here, σ is the number of polymer chains adsorbed per unit area defined by the square of the statistical step length. Using the values of Aharoni¹⁷ of 9.6 Å for the statistical step length and 5.5 for the characteristic ratio of 1,4-polybutadiene, we obtain a mass of 93 g/mol for each statistical step. The critical value of σ is significant because it corresponds to the boundary in the polymer brush scaling diagram at which the polymer brush first begins to become stretched. Below this threshold value, it is possible to increase the number of polymer chains per unit area without perturbing the chain dimensions; so it is reasonable to expect that bringing two particles into close contact is not accompanied by any entropically

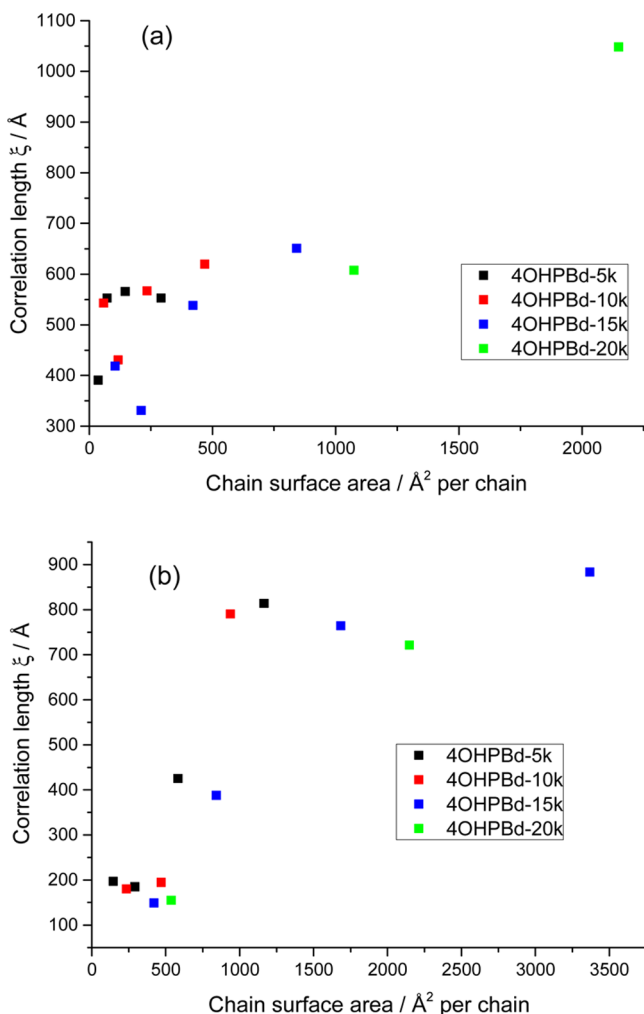


Figure 9. Correlation length versus calculated surface area per adsorbed chain for (a) 5% and (b) 20% silica nanoparticle dispersions.

unfavorable effect on chain dimensions. Conversely, at higher grafting densities, as two coated nanoparticles approach such that the particle–particle surface separation becomes comparable to the dimensions of the adsorbed 4OH-PBd layer, an entropic penalty associated with stretching the chains to accommodate their interdigitation would be incurred. This result is in agreement with the conclusions of Baeza et al.¹³ in their study of grafted SBR silica composites and significantly appears to hold true for several molecular weights of 4OH-PBd. Testing this ansatz for the first time with different molecular weights of grafting polymer puts this result for correlation length versus normalized grafting density beyond doubt, as it eliminates the uncertainty in the scaled grafting density that arises from the unknown prefactor in the brush phase diagram. Interestingly, we find no evidence for aggregation based on autophobic dewetting as observed experimentally^{8,35,36} and predicted in simulations, despite the NR results showing that there can be almost complete exclusion of the matrix from the adsorbed brush layer apparent from the volume fraction profile in Figure 4.

Also of note is that the correlation lengths of the dispersed 5% silica composites are substantially higher than those of the dispersed 20% composite. The reason for this difference could be due to the nature of the correlation length in the model and the concentration of the silica particles. The correlation length,

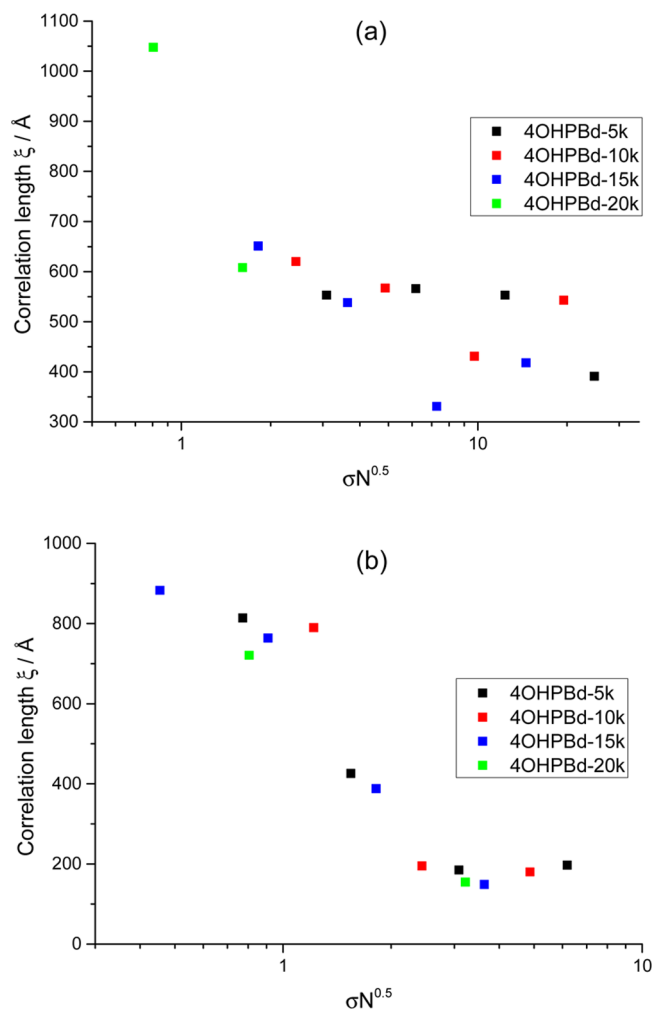


Figure 10. Correlation length versus normalized grafting density for (a) 5% and (b) 20% silica nanoparticle dispersions.

ξ , is the upper limit to which the fractal distribution holds and can be treated as a measure of aggregate size or a particle distribution correlation length. Bearing with the dispersal assumption, below the concentration threshold the silica is aggregated, and the ξ measured relates to the aggregate size, resulting in a similar value between the data sets although with limited points. Once the silica is dispersed, the correlation length measured is that of a particle distribution and is inversely dependent on the concentration of particles. Hence, a greater calculated correlation length in the 5% composites compared with the 20% composites may occur when the particles are dispersed.

Saturated surface thicknesses have been measured from the previous investigation on 4OH-PBd's.¹⁴ The effective layer thickness was used to calculate the chain surface area in a saturated end-functional layer (Table 4). The comparison of

Table 4. Saturated Chain Surface Area for Each 4OH-PBd Estimated from Interfacial Excess Measurements

polymer M_w (g mol ⁻¹)	effective surface thickness, z^* (Å)
6400	94
10300	130
18500	157
23600	159

the SANS results (Table 3) with these values places the critical concentration about 3–6 times lower than the saturation value, which may explain why we do not encounter aggregation driven by autophobic dewetting in these materials. The observed trends can be described by three different regions of scattering behavior dependent on the polymer concentration, visualized in Figure 11. The first region occurs at low 4OH-PBd

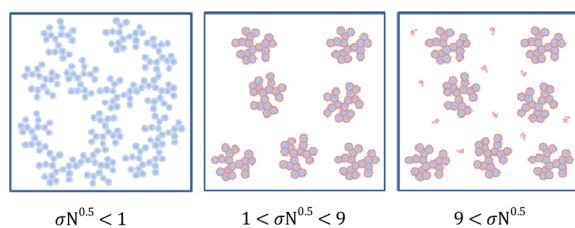


Figure 11. Depiction of a composite sample structure with increasing 4OH-PBd additive concentration, left to right.

concentrations where silica aggregate structures form due to the chains not being able to form adequate polymer layer for steric stability. After a critical polybutadiene surface concentration is reached ($\sigma N^{1/2} \sim 1$) steric stabilization of the silica particles can occur, resulting in the dispersal of the silica into a “hard sphere” primary aggregate arrangement. This breakdown and dispersion of larger aggregates via steric stabilization is in agreement with recent results for carbon black and silica filler systems.^{13,37–39} Eventually, saturation of the end-functional layer results in the buildup of hydrogenated polybutadiene in the matrix, increasing Debye scattering as seen at $Q \sim 0.04 \text{ \AA}^{-1}$ in Figure 6a for 8% and 16% 4OH-PBd.

Rheometry of Nanocomposites. Before considering the filled polymer nanocomposites, we first examine the rheological behavior of the pure matrix material dPBd-90k and that of the end-functional polymer, 4OH-PBd-20k (Figure 8). Despite having only about one-quarter of the molecular weight than the matrix, the end-functional polymer has both higher moduli at low frequency and a slower terminal relaxation time, as evidenced by the lower crossover frequency between G' and G'' . This is the first report of which we are aware concerning the rheology of multi-end-functional polymers, but the result appears to be consistent with earlier SANS studies on related materials, which have shown that there can be a tendency to associate into starlike aggregates polymers.^{26,40} As well as indicating aggregation for 100% end-functional additive, which could not be measured with SANS due to the lack of a contrasting material, the intermediate modulus determined for the PBd + 4OH-PBd blend suggests that dilution with homopolymer does not disrupt the 4OH-PBd aggregates.

For filled rubbers containing both unfunctionalized matrix and 4OH-PBd, some averaging of moduli between the matrix and end-functional polybutadiene is expected by standard rheological theories. Therefore, in the absence of any other effect, we would expect the replacement of dPBd-90k matrix with 4OH-PBd to increase the modulus of the material. The reduction in modulus observed with the addition of 4OH-PBd is therefore significant as it implies some change to the silica distribution (Figure 8c).

Silica filler providing reinforcement to the polymer is well documented, though some contention remains over the exact reasons behind the phenomenon. The rheological results in light of the neutron scattering findings provide evidence for the percolating network theory of reinforcement. The increase in

modulus between the 5% and 20% silica fractions without end-functional polymer is much greater than a simple linear combination of moduli, suggesting some form of structure in the sample. The addition of the end-functional polymer results in a sharp decrease in modulus for the 20% silica sample, while there is less change in the 5% silica sample. The decrease in terminal modulus with “grafted” chains is a new feature, which appears to contradict the behavior reported for styrene–butadiene/silica composites by Baeza et al.¹³ In this earlier study, the adsorbing polymer acted to separate the silica particles from dense, relatively discrete islands of silica toward a more expanded form in which the separation between structures was reduced. In our work, the starting point is that of a silica network, and the addition of adsorbing polymer disrupts this network. We note that the rheology in the presence of adsorbing polymers is qualitatively similar in each case.

The silica volume fraction in both the examined samples is well below the percolation threshold for spheres, 0.28, calculated by computer modeling.⁴¹ Similar reinforcement below this percolation threshold has been reported before and has been partly attributed to the fractal structure of many filler particles resulting in percolation concentrations as low as $\phi \approx 0.033$.^{42–44} Because of this, we theorize that the 20% silica is reinforced by the formation of silica aggregates structures running throughout the matrix and that the breakup of aggregates with end-functional polymer in the composite as seen by small-angle neutron scattering decreases the reinforcement of the polymer matrix and the resultant elastic modulus. At 5% weight fraction a significant network cannot develop due to the scarcity of silica; thus, there is less change with the addition of the 4OH-PBd as the system is already “disperse” and appears to be offset by the higher modulus of the end-functional material. This interpretation would support theories of matrix reinforcement based on the idea of a percolating network structure and at 5% silica loading suggests the presence of more localized aggregate structures that provide reinforcement rather than a large spanning network.

CONCLUSIONS

Through neutron reflectivity we find the preferential adsorption of end-functionalized polybutadiene to silica surfaces in which the matrix is almost completely excluded from the adsorbed brush layer. Small-angle neutron scattering yields evidence for the formation of fractal networks in the silica polybutadiene composites. Furthermore, the addition of end-functionalized polybutadiene was found to spontaneously disperse unmodified silica aggregates to form a more open structure of individual particulates in which the correlation length of the fractal aggregates decreases and the fractal dimension increases. Despite the near exclusion of the matrix from the adsorbed polymer layer, we find no evidence for autophobic dewetting and instead find that the minimum grafting density for effective silica dispersal is unequivocally linked to the transition from mushroom to brushlike behavior in the adsorbed layer structure. For our materials, the enhanced silica dispersal is accompanied by a change in material behavior seen by the decrease in modulus in the samples and demonstrates the large effect a single functional group can have on total molecular and composite behavior. The dispersion of silica and change in moduli provide evidence for percolating network theories of polymer composite reinforcement and suggest that the reinforcement could be more localized than previously thought.

We note that additives of this variety could significantly assist the processing of composite samples without the need for prior surface modification of the filler material.

■ ASSOCIATED CONTENT

● Supporting Information

The Supporting Information is available free of charge on the ACS Publications website at DOI: 10.1021/acs.macromol.5b02318.

Dynamic light scattering results for solution characterization of silica and plots of correlation length as a function of 4OH-PbD additive concentration (PDF)

■ AUTHOR INFORMATION

Corresponding Author

*E-mail r.l.thompson@dur.ac.uk, phone +44 191 334 2139 (R.L.T.).

Present Address

S.M.K.: Synthomer Limited, Central Road, Templefields, Harlow, CM20 2BH, UK.

Notes

The authors declare no competing financial interest.

■ ACKNOWLEDGMENTS

We thank STFC for support of neutron scattering facilities at ISIS and ILL and for support of JMH via Global Futures Scholarship ST/L502625/1. This work benefitted from the use of the SasView application, originally developed under NSF Award DMR-0520547.

■ REFERENCES

- (1) Meera, A. P.; Said, S.; Grohens, Y.; Thomas, S. *J. Phys. Chem. C* **2009**, *113*, 17997.
- (2) Merabia, S.; Sotta, P.; Long, D. R. *Macromolecules* **2008**, *41*, 8252.
- (3) Payne, A. R. *J. Appl. Polym. Sci.* **1963**, *7*, 873.
- (4) Payne, A. R. *J. Appl. Polym. Sci.* **1962**, *6*, 57.
- (5) Basly, B.; Alnasser, T.; Aissou, K.; Fleury, G.; Pecastaings, G.; Hadziioannou, G.; Duguet, E.; Goglio, G.; Mornet, S. *Langmuir* **2015**, *31*, 6675.
- (6) Kim, H.; Abdala, A. A.; Macosko, C. W. *Macromolecules* **2010**, *43*, 6515.
- (7) Napper, D. H. *J. Colloid Interface Sci.* **1977**, *58*, 390.
- (8) Corbierre, M. K.; Cameron, N. S.; Sutton, M.; Laaziri, K.; Lennox, R. B. *Langmuir* **2005**, *21*, 6063.
- (9) Maillard, D.; Kumar, S. K.; Fragneaud, B.; Kysar, J. W.; Rungta, A.; Benicewicz, B. C.; Deng, H.; Brinson, L. C.; Douglas, J. F. *Nano Lett.* **2012**, *12*, 3909.
- (10) Dorigato, A.; Dzenis, Y.; Pegoretti, A. *Mech. Mater.* **2013**, *61*, 79.
- (11) Jouault, N.; Vallat, P.; Dalmas, F.; Said, S.; Jestin, J.; Boue, F. *Macromolecules* **2009**, *42*, 2031.
- (12) Baeza, G. P.; Genix, A. C.; Degrandcourt, C.; Petitjean, L.; Gummel, J.; Couty, M.; Oberdisse, J. *Macromolecules* **2013**, *46*, 317.
- (13) Baeza, G. P.; Genix, A. C.; Degrandcourt, C.; Petitjean, L.; Gummel, J.; Schweins, R.; Couty, M.; Oberdisse, J. *Macromolecules* **2013**, *46*, 6621.
- (14) Kimani, S. M.; Hardman, S. J.; Hutchings, L. R.; Clarke, N.; Thompson, R. L. *Soft Matter* **2012**, *8*, 3487.
- (15) Fetters, L. J.; Lohse, D. J.; Colby, R. H. In *Physical Properties of Polymers Handbook*; Mark, J. E., Ed.; American Institute of Physics: Woodbury, NY, 1996; p 335.
- (16) Stöber, W.; Fink, A.; Bohn, E. *J. Colloid Interface Sci.* **1968**, *26*, 62.
- (17) Aharoni, S. M. *Macromolecules* **1983**, *16*, 1722.
- (18) Kalb, J.; Dukes, D.; Kumar, S. K.; Hoy, R. S.; Grest, G. S. *Soft Matter* **2011**, *7*, 1418.

- (19) Wignall, G. D.; Bates, F. S. *J. Appl. Crystallogr.* **1987**, *20*, 28.
- (20) In Manipulation and Analysis Toolkit for Instrument Data; Mantid Project, 2013.
- (21) Williams, M. L.; Landel, R. F.; Ferry, J. D. *J. Am. Chem. Soc.* **1955**, *77*, 3701.
- (22) Nelson, A. *J. Appl. Crystallogr.* **2006**, *39*, 273.
- (23) Teixeira, J. *J. Appl. Crystallogr.* **1988**, *21*, 781.
- (24) Guinier, A.; Fournet, G. *Small-Angle Scattering of X-rays*; Wiley: New York, 1955.
- (25) Gauthier, C.; Reynaud, E.; Vassoille, R.; Ladouce-Stelandre, L. *Polymer* **2004**, *45*, 2761.
- (26) Ansari, I. A.; Clarke, N.; Hutchings, L. R.; Pillay-Narainan, A.; Terry, A. E.; Thompson, R. L.; Webster, J. R. P. *Langmuir* **2007**, *23*, 4405.
- (27) Bates, F. S.; Wignall, G. D.; Dierker, S. B. *Macromolecules* **1986**, *19*, 1938.
- (28) Schmidt, I.; Binder, K. *J. Phys.* **1985**, *46*, 1631.
- (29) Zink, F.; Kerle, T.; Klein, J. *Macromolecules* **1998**, *31*, 417.
- (30) Balsara, N. P. In *Physical Properties of Polymers Handbook*; Mark, J. E., Ed.; American Institute of Physics: Woodbury, NY, 1996; p 257.
- (31) Lin, M. Y.; Lindsay, H. M.; Weitz, D. A.; Ball, R. C.; Klein, R.; Meakin, P. *Phys. Rev. A: At, Mol., Opt. Phys.* **1990**, *41*, 2005.
- (32) Lin, M. Y.; Lindsay, H. M.; Weitz, D. A.; Ball, R. C.; Klein, R.; Meakin, P. *Nature* **1989**, *339*, 360.
- (33) Lin, M. Y.; Lindsay, H. M.; Weitz, D. A.; Klein, R.; Ball, R. C.; Meakin, P. *J. Phys.: Condens. Matter* **1990**, *2*, 3093.
- (34) Aubouy, M.; Fredrickson, G. H.; Pincus, P.; Raphael, E. *Macromolecules* **1995**, *28*, 2979.
- (35) Hasegawa, R.; Aoki, Y.; Doi, M. *Macromolecules* **1996**, *29*, 6656.
- (36) Sunday, D.; Ilavsky, J.; Green, D. L. *Macromolecules* **2012**, *45*, 4007.
- (37) Baeza, G. P.; Genix, A.-C.; Degrandcourt, C.; Petitjean, L.; Gummel, J.; Schweins, R.; Couty, M.; Oberdisse, J. *Macromolecules* **2013**, *46*, 6621.
- (38) Oberdisse, J.; El Harrak, A.; Carrot, G.; Jestin, J.; Boué, F. *Polymer* **2005**, *46*, 6695.
- (39) Grownay, D. J.; Mykhaylyk, O. O.; Derouineau, T.; Fielding, L. A.; Smith, A. J.; Aragra, N.; Lamb, G. D.; Armes, S. P. *Macromolecules* **2015**, *48*, 3691.
- (40) Kimani, S. M.; Thompson, R. L.; Hutchings, L. R.; Clarke, N.; Billah, S. M. R.; Sakai, V. G.; Rogers, S. E. *Macromolecules* **2014**, *47*, 2062.
- (41) Rintoul, M. D.; Torquato, S. *J. Phys. A: Math. Gen.* **1997**, *30*, L585.
- (42) Jouault, N.; Vallat, P.; Dalmas, F.; Said, S.; Jestin, J.; Boué, F. *Macromolecules* **2009**, *42*, 2031.
- (43) Cassagnau, P. *Polymer* **2003**, *44*, 2455.
- (44) Zhao, D.; Ge, S.; Senses, E.; Akcora, P.; Jestin, J.; Kumar, S. K. *Macromolecules* **2015**, *48*, 5433.